2024 American Control Conference (ACC)
July 8-12, 2024. Toronto, Canada

Sensitivity Analysis of Lithium-ion Battery SoH Indicators: An Analytical Study

Sara Sepasiahooyi and Shu-Xia Tang

Abstract— **The aging processes of lithium-ion (Li-ion) batteries are complex, involving various State-of-Health (SoH) indicators. These mechanisms significantly impact the overall longevity of Li-ion batteries. Sensitivity Analysis (SA) of the terminal voltage to the SoH indicators provides insight into how each aging factor contributes to the battery's lifespan and performance. In this article, SA is applied to six SoH indicators, including, thickness of the Solid Electrolyte Interface (SEI) film in the negative electrode, electrolyte concentration on boundaries, lumped resistance, shell thickness on the positive electrode, volume fraction of active material, and reaction rate constant. Analytical derivation is employed as the SA approach. This generic approach empowers us to apply the results for all current inputs and different types of batteries with various parameters, avoiding data collection and fitting which are typically required in numerical methods. Single Particle Model with electrolyte (SPMe) dynamics is employed as the battery model. The simulation is performed on a Li-ion battery cell with manganese dioxide ($Li_yMn_2O_4$) and carbon (Li_xC_6) as the positive and negative electrode, respectively, and an Urban Dynamometer Driving Schedule (UDDS) current profile.**

Index Terms— **Li-ion Batteries; Sensitivity Analysis; SoH; Aging; SPMe.**

I. Introduction

Having high energy density, Li-ion batteries have been considered as the primary candidate for energy storage applications. Safety and longevity are significant for the performance of batteries. Battery aging mechanisms have a significant impact on various battery parameters, and SoH features are key indicators of this aging process [1]. SA assesses how variations in specific parameters within a system affect changes in the target parameter. SA can be conducted by different methods at various levels of complexity [2]. Many investigations have been conducted on SA of Li-ion battery model parameters. However, there are few SAs dedicated to battery aging metrics. In [3], surrogate Gaussian process regression, which is a machine learning method is used on Doyle–Fuller–Newman (DFN) coupled with an aging battery model for SA on model parameters. In [4], the perturbation approach is applied to determine the SA of battery parameters numerically. In this study, perturbation is already incorporated into the equations during modeling by calculating the derivatives. In [5], analytical derivation is applied for SA on the battery's electrochemical parameters under various current profiles.

In this study, to apply sensitivity of the terminal voltage as the output of the battery, which plays a crucial role in battery estimation and control to the SoH indicators, a Single Particle Model with electrolyte (SPMe) dynamics is employed that yields physically meaningful equations with a high degree of accuracy. This model effectively characterizes the battery aging mechanisms.

The main contributions of this study are as follows:

- Compared with numerical approaches used in previous studies, in this article, the SPMe is employed for analytical SA. To the best of authors' knowledge, an analytical derivation for SA has been applied solely in [5].
- SEI growing film thickness and electrolyte concentration stand as two SoH indicators, and sensitivity of terminal voltage to them is analyzed using an analytical method. To the best of authors' knowledge, no previous reference has explored these aspects analytically.
- Lumped resistance and shell thickness are another SoH indicators that have been considered, and analytical derivations have been applied to analyze them.
- The degradation of the volume fraction of the electrolyte phase ($\varepsilon_e^{\pm}(t)$) and its effects on effective conductivity and diffusivity are considered. However in [5], the volume fraction has been treated as a constant parameter. In this study, the effect of the evolution of the SEI growing film on these parameters is considered.

The remainder of this paper is organized as follows: Section II describes the battery model. In Section III SA of the terminal voltage to the SoH indicators is conducted. Simulation results are shown and discussed in Section IV, followed by a conclusion in Section V.

II. SPMe dynamics

Equivalent Circuit Model (ECM) and electrochemical model are two primary Li-ion battery models. Simplicity of ECM leads to low computational cost for online applications [6]. However, to enhance the analysis of the battery degradation process, this study employs the electrochemical battery model for more effective analysis. The DFN model, an electrochemical model, involves nonlinear partial differential equations, leads to low computational cost for online applications [7]. SPM is a simplified version of the DFN model [8], founded on the assumptions that the electrolyte concentration and potentials are disregarded. These hypotheses come with their limitations; to overcome these constraints, SPMe, depicted in Fig. 1, is employed as the battery model in this paper.

S. Sepasiahooyi and S.-X. Tang (corresponding author) are with the Department of Mechanical Engineering, Texas Tech University, Lubbock, USA. ssepasia@ttu.edu, shuxia.tang@ttu.edu.

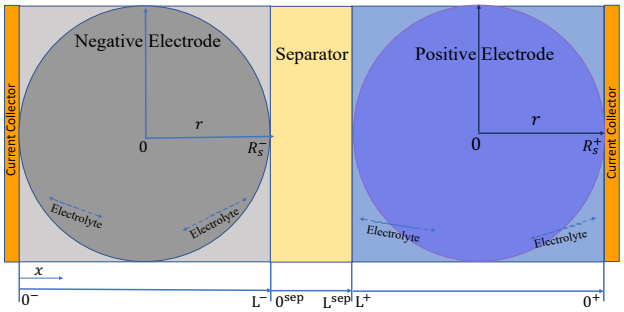

Fig. 1: Schematic of SPMe

A. Solid-phase Li-ion concentration

Solid-phase Li-ion concentration in positive and negative electrodes $(c_s^{\pm}(t,r))$, and the boundary conditions are described as follows:

$$\frac{\partial c_s^{\pm}}{\partial t}(t,r) = \frac{1}{r^2}\frac{\partial}{\partial r}\left[D_s^{\pm} r^2 \frac{\partial c_s^{\pm}}{\partial r}(t,r)\right], t>0, r\in\left(0, R_s^{\pm}\right),$$
$$\frac{\partial c_s^{\pm}}{\partial r}(t,0) = 0, t>0,$$
$$\frac{\partial c_s^{\pm}}{\partial r}(t,R_s^{\pm}) = \pm\frac{1}{D_s^{\pm} a_s^{\pm} F L^{\pm}} I(t), t>0,$$

where r is the radial coordinate, $D_s^{\pm}$ and $L^{\pm}$ are solid phase diffusion coefficient and thickness of the electrodes, respectively. $R_s^{\pm}$ and $a_s^{\pm} = \frac{3\varepsilon_s^{\pm}}{R_s^{\pm}}$ are the the particle radius and the specific interfacial area of the electrodes. $I(t)$ represents the current of the battery as the input to the model. F is the Faraday's constant.

B. Electrolyte concentration

The lithium concentration in the electrolyte within the negative electrode $(c_e^-(t,x))$, separator $(c_e^{\text{sep}}(t,x))$, and positive electrode $(c_e^+(t,x))$ is represented as follows:

$$\frac{\partial c_e^-}{\partial t}(t,x) = \frac{\partial}{\partial x}\left[\frac{D_e^{-,\text{eff}}(c_e^-)}{\varepsilon_e^-}\frac{\partial c_e^-}{\partial x}(t,x)\right] + \frac{(1-t_c^0)}{\varepsilon_e^- F L^-} I(t),$$
$$t>0, x\in\left(0^-, L^-\right) \quad \text{(II.1)}$$
$$\frac{\partial c_e^{\text{sep}}}{\partial t}(t,x) = \frac{\partial}{\partial x}\left[\frac{D_e^{\text{sep,eff}}(c_e^{\text{sep}})}{\varepsilon_e^{\text{sep}}}\frac{\partial c_e^{\text{sep}}}{\partial x}(t,x)\right],$$
$$t>0, x\in(0^{\text{sep}}, L^{\text{sep}}) \quad \text{(II.2)}$$
$$\frac{\partial c_e^+}{\partial t}(t,x) = \frac{\partial}{\partial x}\left[\frac{D_e^{+,\text{eff}}(c_e^+)}{\varepsilon_e^+}\frac{\partial c_e^+}{\partial x}(t,x)\right] - \frac{(1-t_c^0)}{\varepsilon_e^+ F L^+} I(t),$$
$$t>0, x\in\left(L^+,\ 0^+\right), \quad \text{(II.3)}$$

where $D_e^{i,\text{eff}}(c_e^i) = D_e^i(c_e^i).\left(\varepsilon_e^i(t)\right)^{1.5}$, $i\in\{-, sep, +\}$, is the effective diffusivity of electrolyte in separator, positive and negative electrodes, $\varepsilon_e^i(t)$ is the volume fraction of electrolyte and t_c^0 is transference number. Boundary conditions for (II.1),(II.2)and (II.3) are:

$$\frac{\partial c_e^-}{\partial x}(0^-,t) = \frac{\partial c_e^+}{\partial x}(0^+,t) = 0,$$
$$D_e^{-,\text{eff}}(c_e^-(L^-))\frac{\partial c_e^-}{\partial x}(L^-,t) = D_e^{\text{sep,eff}}(c_e(0^{sep}))\frac{\partial c_e^{\text{sep}}}{\partial x}(0^{\text{sep}},t),$$
$$D_e^{\text{sep,eff}}(c_e(L^{\text{sep}}))\frac{\partial c_e^{\text{sep}}}{\partial x}(L^{\text{sep}},t) = D_e^{+,\text{eff}}(c_e(L^+))\frac{\partial c_e^+}{\partial x}(L^+,t),$$
$$c_e^-(L^-,t) = c_e^{\text{sep}}(0^{\text{sep}},t),$$
$$c_e^{\text{sep}}(L^{\text{sep}},t) = c_e^+(L^+,t),$$

where 0^- and 0^+ are the boundaries across the current collectors and L^{sep} is the length of the separator.

C. Terminal voltage

Terminal voltage of battery as the output of system $V(t)$, is derived by the following nonlinear function:

$$V(t) = \left(U^+\left(\frac{c_{\text{ss}}^+(t)}{c_{\text{s}}^{+,\max}}\right) - U^-\left(\frac{c_{\text{ss}}^-(t)}{c_{\text{s}}^{-,\max}}\right)\right) + \left(\varphi_e^+(t,0^+) - \varphi_e^-(t,0^-)\right) + \eta^+(t) + \eta_{\text{shell}}^+(t) - \eta^-(t) - R_\Omega(t)I(t), \quad \text{(II.4)}$$

where $U^{\pm}(.)$ is the Open Circuit Potential (OCP) in electrodes and $c_{ss}^{\pm}(t) = c_s^{\pm}(R_s^{\pm},t)$.

C.1 Electrolyte potential difference

The electrolyte potential difference between the two terminals is obtained as:

$$\varphi_e^+(t,0^+) - \varphi_e^-(t,0^-) \quad \text{(II.5)}$$
$$= \frac{2RT(1-t_c^0)(1+\gamma)}{F}\ln\left(\frac{c_e^+(t,0^+)}{c_e^-(t,0^-)}\right) + \frac{I(t)L^{\text{sep}}}{A\kappa_e^{\text{sep}}(c_e^{\text{sep}}(t,0^{\text{sep}}))(\varepsilon_e^{\text{sep}})^{1.5}} + \frac{I(t)L^+}{2A\kappa_e^+(c_e^+(t,0^+))(\varepsilon_e^+(t))^{1.5}} + \frac{I(t)L^-}{2A\kappa_e^-(c_e^-(t,0^-))(\varepsilon_e^-(t))^{1.5}}, \quad \text{(II.6)}$$

where γ is the activity coefficient, A is the electrode area. $\kappa^{\pm,\text{sep}}(c_e^{\pm,\text{sep}}(t,.))$ is the electrolyte ionic conductivity in the positive, negative electrodes and separator, dependent on electrolyte concentration on boundaries. Note that [5] assumes electrolyte volume fraction as a constant in electrodes and separator; while this paper considers time-varying electrolyte volume fraction, due to its degradation over time. In the negative electrode it is described as [9]:

$$\varepsilon_e^-(t) = 1 - \varepsilon_f^- - \varepsilon_s^-\left(1 + \frac{3L_{\text{SEI}}^-(t)}{R_s^-}\right), \quad \text{(II.7)}$$

and in the positive electrode it is defined as [10]:

$$\varepsilon_e^+(t) = 1 - \varepsilon_f^+ - \varepsilon_s^+, \quad \text{(II.8)}$$

where $\varepsilon_f^{\pm}$ is the volume fraction of the filler, $\varepsilon_s^{\pm}$ is the active material volume fraction and $L_{\text{SEI}}^{\pm}(t)$ is the thickness of SEI film in electrodes. In positive electrode SEI film thickness, L_{SEI}^+ is negligible, so L_{SEI}^+ tends toward zero. Consequently, (II.7) for the positive electrode will undergo a modification to (II.8).

C.2 Overpotential

The overpotential ($\eta^{\pm}(t)$) in (II.4), is given by:

$$\eta^{\pm}(t) = \frac{RT}{\alpha F}\ln\left(\xi^{\pm}(t) + \sqrt{(\xi^{\pm}(t))^2+1}\right), \quad \text{(II.9)}$$
$$\xi^{\pm}(t) = \frac{j^{\pm}(t)}{2a_s^{\pm} i_0^{\pm}(t)},$$

where R represents the universal gas constant. T denotes the temperature of the battery cell, which is assumed to remain constant. Here, intercalation/deintercalation current density $j^{\pm}(t)$, and exchange current density $i_0^{\pm}(t)$, are:

$$j^{\pm}(t) = \mp\frac{I(t)}{a_s^{\pm} F L^{\pm}},$$
$$i_0^{\pm}(t,x) = k^{\pm}\left[c_{ss}^{\pm}(t)\right]^{\alpha_c}\left[c_e^{\pm}(t,x)(c_{s,\max}^{\pm} - c_{ss}^{\pm}(t))\right]^{\alpha_a},$$

where $k^{\pm}$ is the reaction rate constant. In this study an additional term known as shell overpotential $\eta_{\text{shell}}^{+}(t)$, is added to the positive electrode's overpotential, formed during battery aging [11].

C.3 Lumped resistance

The lumped resistance of the battery cell (R_Ω), is expressed as following:

$$R_\Omega(t) = \frac{R_c}{A} + \frac{R_e(t)}{A} + \frac{R_{\text{SEI}}(t)}{A}, \quad \text{(II.10)}$$

where R_c is the resistance of current collectors and wiring. R_e is the electrolyte resistance consisting of three terms associated with separator, negative and positive electrodes:

$$\frac{R_e(t)}{A} = \frac{L^{\text{sep}}}{A\kappa_e^{\text{sep}}(c_e^{\text{sep}}(t,0^{\text{sep}}))(\varepsilon_e^{\text{sep}})^{1.5}} + \frac{L^{-}}{2A\kappa_e^{-,\text{eff}}(c_e^{-}(t,0^{-}))} + \frac{L^{+}}{2A\kappa_e^{+,\text{eff}}(c_e^{+}(t,0^{+}))}, \quad \text{(II.11)}$$

where $\kappa_e^{\text{eff},\pm}(t) = \kappa_e^{\pm}(c_e^{\pm})(\varepsilon_e^{\pm}(t))^{1.5}$ is the electrolyte effective conductivity in electrodes, with consideration of electrolyte volume fraction degradation in (II.7) and (II.8).

In [5], $R_{\text{SEI}}^{\pm}(t)$ is considered constant, However in this study the evolution of SEI resistance is considered through the growing SEI film thickness. In this study, the resistance of SEI growing film is considered as follows [12]:

$$\frac{R_{\text{SEI}}(t)}{A} = \frac{L_{\text{SEI}}^{+}(t)}{AL^{+}a_s^{+}\kappa_{\text{SEI}}} + \frac{L_{\text{SEI}}^{-}(t)}{AL^{-}a_s^{-}\kappa_{\text{SEI}}}, \quad \text{(II.12)}$$

where κ_{SEI} is the ionic conductivity of SEI film.

III. SoH indicators and sensitivity analysis

A. SEI growing film

A.1 SEI growing film composition and effects

The SEI growing film leads to battery resistance growth and ohmic potential drop on the battery terminal voltage. SEI film will grow on both electrodes. However, due to its notably thin presence on the positive electrode, the sensitivity of voltage to SEI film thickness is exclusively focused on the negative electrode.

A.2 SA of terminal voltage to SEI growing film

According to (II.4), the thickness of SEI film in the negative electrode L_{SEI}^{-}, impacts the terminal voltage of battery through the electrolyte potential difference $\Delta\varphi_e$, the electrolyte resistance $R_e(t)$, and SEI resistance $R_{\text{SEI}}(t)$.

$$\frac{\partial V(t)}{\partial L_{\text{SEI}}^{-}(t)} = \frac{\partial \Delta\varphi_e(c_e^{-}(0^{-},t))}{\partial L_{\text{SEI}}^{-}(t)} - \frac{\partial R_e^{-}(t)}{\partial L_{\text{SEI}}^{-}(t)} I(t) - \frac{\partial R_{\text{SEI}}^{-}(t)}{\partial L_{\text{SEI}}^{-}(t)} I(t). \quad \text{(III.1)}$$

A.2.1 SEI thickness effect on the electrolyte potential

$\frac{\partial \Delta\varphi_e(c_e^{-}(0^{-},t))}{\partial L_{\text{SEI}}^{-}(t)}$ describes the impact of SEI thickness on the electrolyte potential. In [5], the diffusion coefficient $D_e^{\text{eff},-} = D_e^{-}\varepsilon_e^{1.5}$, is treated as a constant parameter. However, in this study, the degradation of electrolyte volume fraction in negative electrode is considered as [9]:

$$D_e^{-,\text{eff}}(t) = D_e^{-}\left[1 - \varepsilon_f^{-} - \varepsilon_s^{-}(1 + \frac{3L_{\text{SEI}}^{-}(t)}{R_s^{-}})\right]^{1.5}. \quad \text{(III.2)}$$

By applying the chain rule differentiation, partial derivative of $\Delta\varphi_e(c_e^{-}(t,0^{-}))$ to $L_{\text{SEI}}^{-}(t)$ can be extended as:

$$\frac{\partial \Delta\varphi_e(c_e^{-}(t,0^{-}))}{\partial L_{\text{SEI}}^{-}(t)} = \frac{\partial \Delta\varphi_e(c_e^{-}(t,0^{-}))}{\partial c_e^{-}(t,0^{-})} \times \frac{\partial c_e^{-}(t,0^{-})}{\partial D_e^{-,\text{eff}}(c_e^{-}(t,0^{-}), L_{\text{SEI}}^{-}(t))} \times \frac{\partial D_e^{-,\text{eff}}(c_e^{-}(t,0^{-}), L_{\text{SEI}}^{-}(t))}{\partial L_{\text{SEI}}^{-}(t)}. \quad \text{(III.3)}$$

From (II.6), first term of (III.3) is derived as

$$\frac{\partial \Delta\varphi_e(c_e^{-}(t,0^{-}))}{\partial c_e^{-}(t,0^{-})} = \frac{-2RT(1-t_c^0)}{Fc_e^{-}(t,0^{-})}(1+\gamma). \quad \text{(III.4)}$$

For second term of (III.3), sensitivity transfer function from [5, Section 4.4] is employed. The last terms of (III.3) can be derived as follows:

$$\frac{\partial D_e^{-,\text{eff}}(c_e^{-}(t,0^{-}), L_{\text{SEI}}^{-}(t))}{\partial L_{\text{SEI}}^{-}(t)} = \frac{-4.5D_e^{-}(c_e^{-}(t,0^{-}))\varepsilon_s^{-}}{R_s^{-}} \times \left[1 - \varepsilon_f^{-} - \varepsilon_s^{-}\left(1 + \frac{3L_{\text{SEI}}^{-}(t)}{R_s^{-}}\right)\right]^{0.5}. \quad \text{(III.5)}$$

A.2.2 SEI thickness effect on the electrolyte resistance

The second term in (III.1), $\frac{\partial R_e(t)}{\partial L_{\text{SEI}}^{-}(t)} I(t)$, reflects the effect of SEI film thickness on the terminal voltage via electrolyte resistance. From (II.11), it can be derived that:

$$\frac{\partial R_e(\kappa_e^i(c_e^i(t,0^{-}), L_{\text{SEI}}^{\pm}(t)))}{\partial L_{\text{SEI}}^{-}(t)} I(t) = \frac{2.25L^{-}\varepsilon_s^{-} I(t)}{A\kappa_e^{-}(c_e^{-})R_s^{-}}\left[1 - \varepsilon_f^{-} - \varepsilon_s^{-}\left(1 + \frac{3L_{\text{SEI}}^{-}(t)}{R_s^{-}}\right)\right]^{-2.5}.$$

A.2.3 SEI thickness effect on the SEI resistance

The third term in (III.1), $\frac{\partial R_{\text{SEI}}(t)}{\partial L^{-}_{\text{SEI}}(t)}$, shows the impact of SEI film thickness on voltage through SEI resistance:

$$\frac{\partial R_{\text{SEI}}(t)}{\partial L^{-}_{\text{SEI}}(t)} = \frac{I(t)}{AL^{-}a_s^{-}\kappa_{\text{SEI}}}. \tag{III.6}$$

To conclude, from (III.3) to (III.6), the partial derivation of terminal voltage to SEI thickness L^{-}_{SEI}, is a linear function of current $I(t)$, and a nonlinear function of lithium concentration in negative electrode $c_e^{-}(t)$, and SEI layer thickness.

B. Electrolyte Concentration on boundaries

The electrolyte concentration changes with aging, hence it can be used as a SoH indicator [13]. Partial derivation of $V(t)$ to the electrolyte concentration on boundaries ($c_e(t,0^{\pm})$ is:

$$\frac{\partial V(t)}{\partial c_e^{\pm}(t,0^{\pm})} = \frac{\partial \phi_e^{\pm}(t)}{\partial c_e(t,0^{\pm})} - \frac{\partial R_e(t)}{\partial c_e^{\pm}(t,0^{\pm})} I(t) = \frac{-L^{\pm})}{2A\kappa^{-,\text{eff}}(c_e^{\pm}(t,0^{\pm}))^2} \frac{\partial k^{\pm,\text{eff}}(c_e^{-}(t,0^{\pm})}{\partial c_e^{\pm}(t,0^{\pm})} - \frac{\partial R_e(t)}{\partial c_e^{\pm}(t,0^{\pm})} I(t).$$

C. Lumped resistance

As a battery ages, changes in the electrodes and electrolyte lead to an increase in its internal resistance. The lumped resistance is proportional to the current, so from (II.10):

$$\frac{\partial V(t)}{\partial R_{\Omega}(t)} = -I(t).$$

D. Shell thickness

The phase transition and structural changes occurring in the spinel/rock-salt phase, which only exist in the positive electrode, are assumed to manifest as a shell. Some of the cyclable Li-ions will be trapped within this shell, resulting in loss of active material. The resistance of shell layer is expressed as follows [11]:

$$R^{+}_{\text{shell}}(t) = \frac{\rho^{+}_{\text{shell}} L^{+}_{\text{shell}}(t)}{A},$$

where ρ^{+}_{shell} is the shell resistivity which is assumed to be constant and uniform and $L^{+}_{\text{shell}}(t)$ is the thickness of shell. The overpotential across the shell formulated as:

$$\eta^{+}_{\text{shell}}(t) = R^{+}_{\text{shell}}(t) I(t) = \frac{\rho^{+}_{\text{shell}} L^{+}_{\text{shell}}(t)}{A} I(t).$$

Based on (II.4), the shell resistance impacts the terminal voltage of battery cell via the shell overpotential $\eta^{+}_{\text{shell}}(t)$. Hence the sensitivity of shell resistance in positive electrode to the terminal voltage of battery is the following linear function of current $I(t)$:

$$\frac{\partial V(t)}{\partial L^{+}_{\text{shell}}(t)} = \frac{\partial \eta^{+}_{\text{shell}}(t)}{\partial L^{+}_{\text{shell}}(t)} = \frac{\rho^{+}_{\text{shell}} I(t)}{A}.$$

E. Active material volume fraction

The active material volume fraction in solid phase ($\varepsilon_s^{\pm}$), impacts the terminal voltage via SEI film resistance, overpotential and OCP. By applying the chain rule, the sensitivity of terminal voltage to $\varepsilon_s^{\pm}$ is derived as [5, Section 4.2]:

$$\frac{\partial V(t)}{\partial \varepsilon_s^{\pm}} = \frac{\partial R^{\pm}_{\text{SEI}}(t)}{\partial \varepsilon_s^{\pm}} I(t) + \frac{\partial \eta^{\pm}(t)}{\partial a_s^{\pm}} \frac{\partial a_s^{\pm}}{\partial \varepsilon_s^{\pm}} + \left(\frac{\partial \eta^{\pm}(t)}{\partial c_{ss}^{\pm}(t)} + \frac{\partial U^{\pm}(t)}{\partial c_{ss}^{\pm}(t)} \right) \frac{\partial c_{ss}^{\pm}(t)}{\partial \varepsilon_s^{\pm}} = \frac{-L^{\pm}_{\text{SEI}}(t) R_s^{\pm}}{3AL^{\pm}(\kappa^{\pm}_{\text{SEI}}(\varepsilon_s^{+}))^2} I(t) - \frac{RT}{\alpha F \varepsilon_s^{\pm}} \frac{\text{sign}(I(t))}{\sqrt{1 + \left(\frac{6\varepsilon_s^{\pm} i_0^{\pm}(t) AL^{i}}{I(t) R_s^{\pm}} \right)^2}} + \left(\frac{\partial \eta^{\pm}(t)}{\partial c_{ss}^{\pm}(t)} + \frac{\partial U^{\pm}(t)}{\partial c_{ss}^{\pm}(t)} \right) \frac{\partial c_{ss}^{\pm}(t)}{\partial \varepsilon_s^{\pm}}.$$

$\frac{\partial \eta^{\pm}(t)}{\partial c_{ss}^{\pm}(t)}$ is derived in [5, Section 4.1]. $\frac{\partial U^{\pm}(t)}{\partial c_{ss}^{\pm}(t)}$ is the slope of the OCV. For $\frac{\partial c_{ss}(t)}{\partial \varepsilon_s^{\pm}}$, by using the transcendental transfer function ($\frac{C_s^{\pm}(s)}{I(s)}$) from [5] and 5th order Padé approximation result by using WolframAlpha, the partial derivative with respect to $\varepsilon_s^{\pm}$ is obtained as:

$$\frac{\partial C_s^{\pm}}{\partial \varepsilon_s^{\pm}}(s) = \frac{-R_s^{\pm} I(s)}{3F(\varepsilon_s^{\pm})^2 AL^{\pm}} \times P_c(s),$$

where $P_c(s) =$

$$\frac{-\frac{(R_s^{\pm})^7 s^4}{3968055(D_s^{\pm})^4} - \frac{4(R_s^{\pm})^5 s^3}{33915(D_s^{\pm})^3} - \frac{21(R_s^{\pm})^3 s^2}{1615(D_s^{\pm})^2} - \frac{8(R_s^{\pm})s}{19D_s^{\pm}} - \frac{3}{R_s^{\pm}}}{\frac{(R_s^{\pm})^8 s^5}{218243025(D_s^{\pm})^4} + \frac{2(R_s^{\pm})^6 s^4}{305235(D_s^{\pm})^3} + \frac{3(R_s^{\pm})^4 s^3}{2261(D_s^{\pm})^2} + \frac{7(R_s^{\pm})^2 s^2}{95D_s^{\pm}} + s}.$$

Sensitivity of terminal voltage to the active material volume fraction, $\varepsilon_s^{\pm}$, is linear and nonlinear functions of current and lithium concentration in the electrodes and electrolyte on the boundaries.

F. Reaction rate constant

Reaction rate constant refers to the velocity at which chemical processes take place within a battery during the charging and discharging phases. The effect of the reaction rate constant $k^{\pm}$, on the terminal voltage is exclusively through the over-potential $\eta^{\pm}(t)$. Thus [5, Section 4.3]:

$$\frac{\partial V(t)}{\partial k^{\pm}} = \frac{\partial \eta^{\pm}(t)}{\partial \xi^{\pm}(t)} \frac{\partial \xi^{\pm}(t)}{\partial k^{\pm}} = \frac{-RT}{\alpha^{\pm} F k^{\pm}} \frac{\text{sign}(I(t))}{\sqrt{1 + (\frac{6\varepsilon_s^{\pm} i_0^{\pm} AL^{\pm}}{I(t) R_s^{\pm}})^2}}.$$

IV. Simulation

The simulation is performed on a battery cell with manganese dioxide ($\text{Li}_y\text{Mn}_2\text{O}_4$) and carbon ($\text{Li}_x\text{C}_6$) as positive and negative electrodes, respectively; with rated capacity of 2700mAh. The temperature is assumed to be constant at T = 298 [K]. The electrochemical parameters of battery model are extracted from [14], [11], and [12]. Ionic conductivity function and OCP are from [15]. the UDDS current profile shown in Fig. 2 is utilized as the input current to the battery. In this simulation, the 5th order Padé approximation is utilized. As demonstrated in [16], comparing the results of

the PDE with the 3rd order Padé approximation reveals their proximity. Employing the 5th order Padé approximation in this simulation ensures a closer match to the original system, resulting in more precise outcomes.

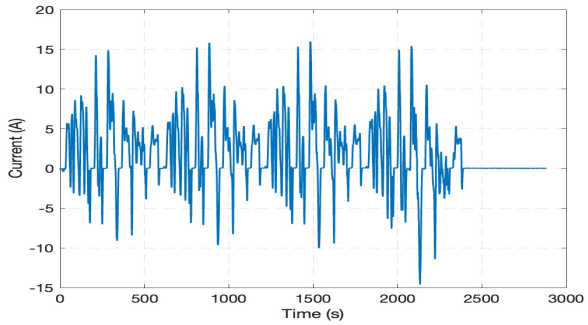

Fig. 2: UDDS profile

For having comparable scales for the results, all sensitivity values have been normalized, with an example being the normalization of L_{SEI}^{-} as [17]:

$$S_{L_{\text{SEI}}^{-}}^{\text{normalized}} = \frac{\partial V(t)}{\partial L_{\text{SEI}}^{-}(t)} \times \frac{L_{\text{SEI}}^{-,*}}{V^{*}},$$

where $*$ denotes the nominal value of the parameters, which are as follows: $V^{*} = 3.6$v, $R_{\Omega}^{*} = 1.5 \times 10^{-4}\Omega$, $k^{+,*}$=2.3×10^{-4}, $k^{-,*}$=7.5×10^{-5}, $c_e^{*}(0,x)$=1000, $L_{\text{SEI}}^{-,*}$ =20nm [12], $L_{\text{shell}}^{+,*} = 4.5 \times 10^{-8}$m, $\varepsilon_s^{-,*}$=0.694 [11].

SA of voltage to SEI growing film in the negative electrode $L_{\text{SEI}}^{-}(t)$, is presented in Fig. 3. Notably, it becomes apparent that SEI thickness has not a significant impact in this plot. This phenomenon can be attributed to the fact that in the initial stages, the thickness of SEI film has a stabilizing effect and is relatively negligible. However, as the battery ages, the degradation effect of SEI becomes more pronounced and evolves into one of the primary factors.

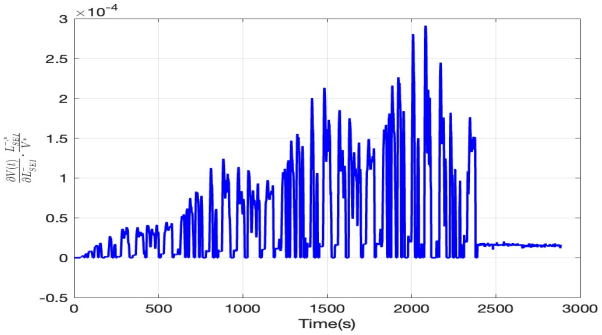

Fig. 3: Sensitivity of voltage to SEI growing film thickness in the negative electrode

SA of voltage to the lumped resistance is illustrated in Fig. 4. In Fig. 5, sensitivity of voltage to electrolyte concentration in negative electrode boundary is plotted which its trend is different from the other plots, because it is not related to the current of battery and only depends on the electrolyte concentration. The impact of shell resistance on the terminal voltage in the positive electrode is illustrated in Fig. 6. It can be observed that it has a notable influence on the terminal voltage among the various factors. SA of voltage to the active material volume in negative electrode is displayed in Fig. 7. The results reveal that active material volume has

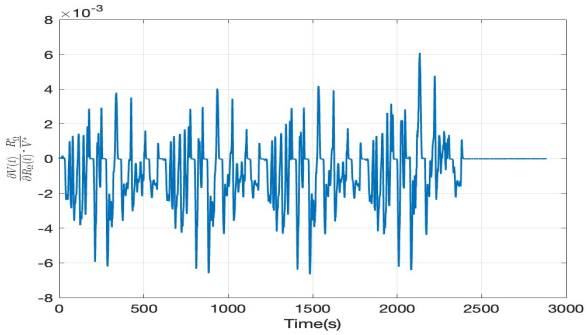

Fig. 4: Sensitivity of voltage to the lumped resistance $R_{\Omega}(t)$

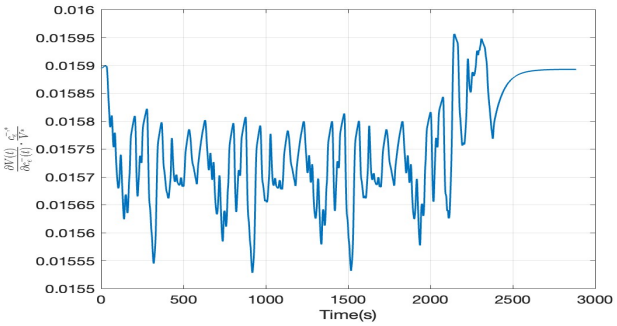

Fig. 5: Sensitivity of voltage to $c_e^{-}(t,0^{-})$

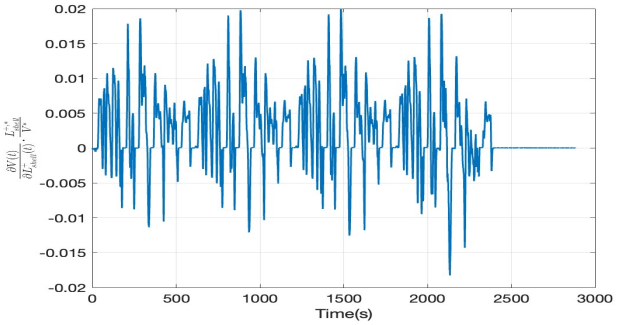

Fig. 6: Sensitivity of voltage to the shell resistance

the most significant influence on the terminal voltage. This observation aligns with the analytical derivative presented in (III.1), because it affects a greater number of components in the terminal voltage, while other parameters impact only one or two. Sensitivity of voltage to the reaction rate constant

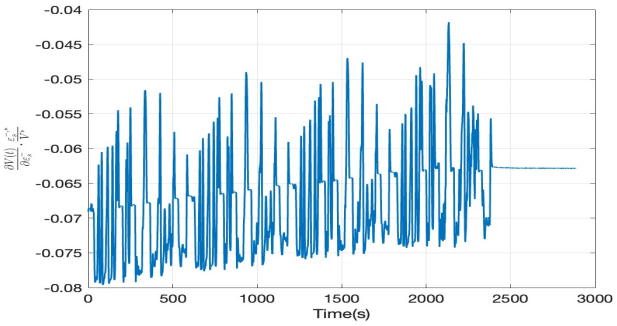

Fig. 7: Sensitivity of voltage to the active material volume fraction in the negative electrode

in positive and negative electrodes are illustrated in Fig. 8 and Fig. 9. The plots reveal that positive electrode has a greater effect than negative electrode on voltage. This difference arises from the fact that the positive electrode contains a higher proportion of active material participating

in chemical reactions compared to the negative electrode resulting simulation on manganese dioxide battery. It has

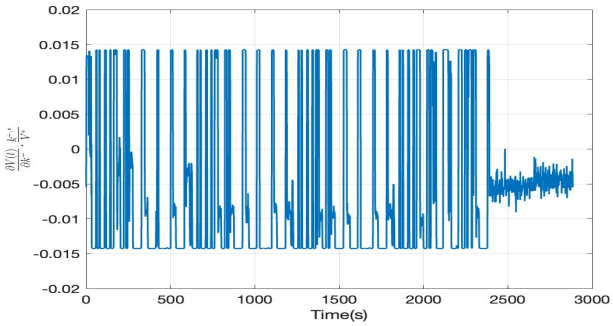

Fig. 8: Sensitivity of voltage to reaction rate in positive electrode

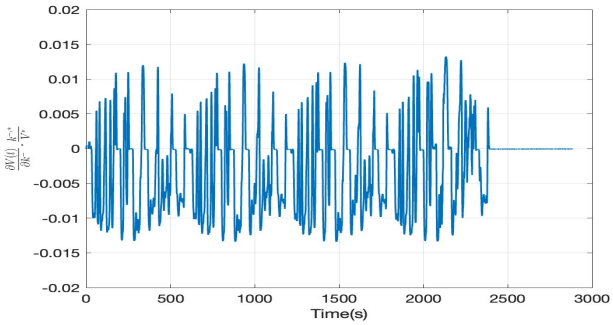

Fig. 9: Sensitivity of voltage to reaction rate in negative electrode

been identified that the voltage of the battery cell is most sensitive to electrolyte concentration, volume fraction of active material, and reaction rate constant. Therefore the new SoH indicators vector is described as:

$$\text{SoH} = \begin{bmatrix} c_e(t, 0^{\pm}) & \varepsilon_s & k \end{bmatrix}^T.$$

While the SEI thickness and lumped resistance have a comparatively minor impact. These effects become more pronounced as the battery ages over time. However, during the initial stages, they exhibit a relatively smaller impact on the terminal voltage, as the simulation focuses on the early phase of battery life.

V. Conclusion and Future Works

In this study, SA is conducted for six SoH indicators, which include SEI film in the negative electrode, electrolyte concentration on boundaries, lumped resistance, shell thickness in the positive electrode, active material volume fraction and reaction rate constant, which can be extended to more SoH metrics such as state of charge. In future research we will incorporate the most effective identified SoH indicators in this study for SoH estimation and SoH fault detection schemes. The presented results are derived from simulations conducted on the specified type of battery. While these findings may vary for other types of batteries. However, the general applicability of this approach allows us to apply it to the battery cells with alternative materials and different current profiles as the future work. In addition finite difference method for PDE simulation and compare with Padé approximation reult can be done in the future.

Acknowledgments

The authors would like to acknowledge Professor Xinfan Lin for discussing some technical details.

References

[1] Vahid Safavi, Najmeh Bazmohammadi, Juan C Vasquez, and Josep M Guerrero. Battery state-of-health estimation: A step towards battery digital twins. *Electronics*, 13(3):587–609, 2024.

[2] Bertrand Iooss and Paul Lemaître. A Review on Global Sensitivity Analysis Methods. *Uncertainty Management in Simulation-Optimization of Complex Systems*, 59:pp. 101–122, 2015.

[3] Mohammad Alipour, Litao Yin, Shiva Sander Tavallaey, Anna Mikaela Andersson, and Daniel Brandell. A surrogate-assisted uncertainty quantification and sensitivity analysis on a coupled electrochemical–thermal battery aging model. *Journal of Power Sources*, 579:233–273, 2023.

[4] Saehong Park, Dylan Kato, Zach Gima, Reinhardt Klein, and Scott Moura. Optimal experimental design for parameterization of an electrochemical lithium-ion battery model. *Journal of The Electrochemical Society*, 165(7):A1309–A1323, 2018.

[5] Qingzhi Lai, Sidharth Jangra, Hyoung Jun Ahn, Geumbee Kim, Won Tae Joe, and Xinfan Lin. Analytical derivation and analysis of parameter sensitivity for battery electrochemical dynamics. *Journal of Power Sources*, 472:228–338, 2020.

[6] Sepasiahooyi Sara and Farzaneh Abdollahi. Fault Detection of New and Aged Lithium-ion Battery Cells in Electric Vehicles. In *2022 8th International Conference on Control, Instrumentation and Automation (ICCIA)*, pages 1–5, 2022.

[7] Guangwei Chen, Zhitao Liu, Hongye Su, and Weichao Zhuang. Electrochemical-distributed thermal coupled model-based state of charge estimation for cylindrical lithium-ion batteries. *Control Engineering Practice*, 109:1–8, 2021.

[8] Shu-Xia Tang, Leobardo Camacho-Solorio, Yebin Wang, and Miroslav Krstic. State-of-charge estimation from a thermal–electrochemical model of lithium-ion batteries. *Automatica*, 83:206–219, 2017.

[9] Eric Prada, D Di Domenico, Y Creff, J Bernard, Valérie Sauvant-Moynot, and François Huet. A simplified electrochemical and thermal aging model of LiFePO4-graphite Li-ion batteries: Power and capacity fade simulations. *Journal of The Electrochemical Society*, 160(4):A616–A628, 2013.

[10] Godfrey Sikha, Branko N Popov, and Ralph E White. Effect of Porosity on the Capacity Fade of a Lithium-Ion Battery: Theory. *Journal of The Electrochemical Society*, 151(7):A1104–A1114, 2004.

[11] Mingzhao Zhuo, Gregory Offer, and Monica Marinescu. Degradation model of high-nickel positive electrodes: Effects of loss of active material and cyclable lithium on capacity fade. *Journal of Power Sources*, 556:232–461, 2023.

[12] Frank M Kindermann, Jonas Keil, Alexander Frank, and Andreas Jossen. A SEI modeling approach distinguishing between capacity and power fade. *Journal of The Electrochemical Society*, 164(12):E287–E294, 2017.

[13] Lena Spitthoff, Paul R Shearing, and Odne Stokke Burheim. Temperature, ageing and thermal management of lithium-ion batteries. *Energies*, 14(5):1248–1278, 2021.

[14] Shifei Yuan, Lei Jiang, Chengliang Yin, Hongjie Wu, and Xi Zhang. A transfer function type of simplified electrochemical model with modified boundary conditions and Padé approximation for Li-ion battery: Part 1. lithium concentration estimation. *Journal of Power Sources*, 352:245–257, 2017.

[15] Chang-Hui Chen, Ferran Brosa Planella, Kieran O'regan, Dominika Gastol, W Dhammika Widanage, and Emma Kendrick. Development of Experimental Techniques for Parameterization of Multi-scale Lithium-ion Battery Models. *Journal of The Electrochemical Society*, 167(8):1–23, 2020.

[16] Shifei Yuan, Lei Jiang, Chengliang Yin, Hongjie Wu, and Xi Zhang. A transfer function type of simplified electrochemical model with modified boundary conditions and padé approximation for li-ion battery: Part 1. lithium concentration estimation. *Journal of Power Sources*, 352:245–257, 2017.

[17] Jakob Kirch, Caterina Thomaseth, Antje Jensch, and Nicole E Radde. The effect of model rescaling and normalization on sensitivity analysis on an example of a MAPK pathway model. *EPJ Nonlinear Biomedical Physics*, 4(1):1–23, 2016.